Relativistic distorted-wave cross sections for electron-impact excitations of berylliumlike ions

Wen-Jia Qian* and Yong-Ki Kim
National Institute of Standards and Technology, Gaithersburg, Maryland 20899

Jean-Paul Desclaux
Serivce de Physique, Département de Recherche Fondamentale, Centre d'Etudes Nucléaires de Grenoble, 38041 Grenoble CEDEX, France

(Received 28 November 1988)

Relativistic distorted-wave Born (RDWB) cross sections of Be-like ions for excitations from the ground state $2s^2\,{}^1S_0$ to the $2s2p\,{}^3P_1$ and ${}^1P_1$ states by electron impact are reported for Ne^{6+} through U^{88+}. Multiconfiguration Dirac-Fock wave functions were used to describe the target-ion states, and the relativistic continuum wave functions were calculated in the field of (frozen) target-ion charge distribution with the configuration-average exchange potential. We found, however, that cross sections hardly changed even if the exchange terms were omitted. In contrast, adding the $2p^2$ configuration to the ground-state wave function reduced cross sections by 10–60%. RDWB cross sections were calculated from thresholds to $T=10$ keV, where T is the incident electron energy. For $Z\simeq 25$ and above, where Z is the nuclear charge, intermediate coupling mixes the ${}^3P_1$ and ${}^1P_1$ states such that the transition to the former becomes practically spin- and electric-dipole allowed, changing the high-T behavior of the excitation cross section. Cross sections are presented in compact fitting formulas that allow interpolations to determine cross sections with high precision for arbitrary Be-like ions ($10\le Z\le 92$) and arbitrary incident energies ($T\le 10$ keV).

I. INTRODUCTION

Relativistic effects in excitation and ionization of atoms (and ions) arise from two main sources: relativistic effects in target-atom wave functions and those from the relativistic interaction of the incident and bound electrons in the target atom.[1] The former manifests itself for heavy atoms and highly charged ions even when the incident electron is slow, while the latter appears through relativistic kinematics and relativistic electron-electron interaction known as Møller scattering[2] when the incident electron energy approaches or exceeds the electron rest mass. Therefore, for applications that require cross sections of highly charged ions, such as fusion reactor modeling and x-ray laser design, it is essential that relativistic wave functions are used in describing the charge density of target ions. Then, it is natural to use relativistic continuum wave functions for consistency and simpler logic in describing electron-impact excitation of highly charged ions, although the incident energy T may not be high enough to make the Møller scattering between the incident and bound electrons significant. Our theoretical approach is similar to that used by Hagelstein,[3] although the wave function codes used by Hagelstein and by us are different in many aspects. Our bound-state wave-function code is an improved version of that reported earlier by one of us.[4]

In this article we present relativistic distorted-wave Born (RDWB) cross sections for electron-impact excitations of Be-like ions from the ground state $2s^2\,{}^1S_0$ to the $2s2p\,{}^3P_1$ and ${}^1P_1$ states. These cross sections are well suited to demonstrate (a) the effect of electron correlation in the target ions, (b) the effect of intermediate coupling, and (c) the possibility of condensing the vast amount of cross-section data into compact formulas whose fitted constants are expressed in terms of simple functions of atomic numbers Z. These formulas contain a total of 81 constants to accurately reproduce the original RDWB cross sections for every ion between $Z=10$ and 92 at any incident energy $T\le 10$ keV.

A brief description of bound and continuum wave functions used in the present work is given in Sec. II. The dependence of cross sections on T and Z along with fitting formulas used are described in Secs. III and IV. Our results are compared with other theoretical data in Sec. V, and conclusions are presented in Sec. VI.

II. THEORY

It is well known that the ground state of Be-like ions requires a correlated description of its charge density; at least a mixture of $2s^2$ and $2p^2$ in nonrelativistic notation should be used.[5] We used a multiconfiguration Dirac-Fock (MCDF) wave function that includes $2s^2$, $2p_{1/2}^2$, and $2p_{3/2}^2$ configurations for the ${}^1S_0$ ground state, and MCDF wave functions that include $2s2p_{1/2}$ and $2s2p_{3/2}$ configurations for the ${}^3P_1$ and ${}^1P_1$ states

$$\Psi(J=0)=a\,\psi(2s^2)+b\,\psi(2p_{1/2}^2)+c\,\psi(2p_{3/2}^2)\ , \tag{1}$$

and

$$\Phi(J=1)=a'\phi(2s2p_{1/2})+b'\phi(2s2p_{3/2})\ , \tag{2}$$

where a, b, c, a', and b' are configuration mixing

coefficients, which are variationally determined. The lower $J=1$ state corresponds to the $^3P_1$ state, and the upper one to the $^1P_1$ state. Both Ψ and Φ include a K-shell core which we omitted in Eqs. (1) and (2) for brevity.

Intermediate coupling in the two $J=1$ states is introduced by allowing the configuration mixing coefficients to be determined variationally. For low-Z ions, the mixing coefficients (a',b') are close to the LS-coupling limits of $(\sqrt{2/3},\sqrt{1/3})$ and $(-\sqrt{1/3},\sqrt{2/3})$, thus making the lower $J=1$ state almost a pure ^3P state and the upper one a pure ^1P state. As Z increases, these mixing coefficients gradually depart from the LS-coupling limit and approach the jj-coupling limits of (1,0) and (0,1) (see Table I).

In the usual MCDF method, all orbitals and mixing coefficients both of the initial and final states are determined by allowing them to vary freely. Such a procedure produces the best excitation energies and charge distributions. The resulting orbitals of Ψ and Φ, however, are not orthonormal to each other, i.e., the $2p_{1/2}$ orbital of Ψ is not the same as the $2p_{1/2}$ orbital of Φ, nor the $2s$ orbital of Ψ orthogonal to the $1s$ orbital of Φ.

The expressions for interaction matrix elements that allow for the nonorthogonality of initial- and final-state orbitals are too cumbersome for practical applications, particularly with multiconfiguration wave functions. To avoid this complexity, we have used the same core orbitals for Ψ and Φ, although excitation energies were determined by using fully variational orbitals both for the initial and final states.

The continuum orbitals of a given Dirac angular quantum number κ were forced to be orthogonal to bound-state orbitals of the same κ by introducing Lagrange multipliers in the Dirac-Fock equations satisfied by the continuum orbitals. We did not, however, enforce orthogonality between the continuum orbitals of the incoming electron and those of the outgoing electron; they were determined separately, the former in the field of the initial-state charge distribution of the target ion and the latter in the field of the final-state charge distribution. Exchange with the core electrons of the target ion was treated by using the average-configuration (in jj coupling) exchange, i.e., the exchange potential was explicitly included in the Dirac-Fock equation for the partial waves, similar to bound-state Dirac-Fock calculations.

Moreover, in view of the fact that the $2p$ orbitals of the $2s2p$ ^3P and ^1P states are rather different,[6] the $2p_j$ orbitals for the lower and upper $J=1$ states were determined separately and used in matching ground-state wave functions. In other words, the Ψ used with the lower $J=1$ state had different $2p_j$ orbitals than those in the Ψ used with the upper $J=1$ state. We present in Table I examples of configuration mixing coefficients and excitation

TABLE I. Energies and configuration-mixing coefficients of Be-like ions. ($2s=2s_{1/2}$, $2p^*=2p_{1/2}$, $2p=2p_{3/2}$.)

Ion	Configuration-mixing coefficient: Relaxed orbitals	$^3P_1$, frozen orbitals	$^1P_1$, frozen orbitals	Excitation energy (eV): Relaxed orbitals	Frozen orbitals
Ne^{6+}					
$^1S_0$ $2s^2$	0.967 71	0.967 69	0.968 08		
$2p^{*2}$	0.146 54	0.146 58	0.145 69		
$2p^2$	0.205 09	0.205 15	0.203 94		
$^3P_1$ $2s2p^*$	0.820 35	0.820 36		14.07	14.00
$2s2p$	0.571 86	0.571 85			
$^1P_1$ $2s2p^*$	−0.571 72		−0.571 85	28.29	28.29
$2s2p$	0.820 45		0.820 36		
Xe^{50+}					
$^1S_0$ $2s^2$	0.988 91	0.988 88	0.989 26		
$2p^{*2}$	0.138 26	0.138 47	0.135 76		
$2p^2$	0.054 21	0.054 23	0.054 10		
$^3P_1$ $2s2p^*$	0.994 82	0.994 80		128.11	128.19
$2s2p$	0.101 69	0.101 80			
$^1P_1$ $2s2p^*$	−0.101 56		−0.101 81	533.70	533.66
$2s2p$	0.994 83		0.994 80		
U^{88+}					
$^1S_0$ $2s^2$	0.993 52	0.993 51	0.995 98		
$2p^{*2}$	0.112 99	0.113 02	0.088 64		
$2p^2$	0.012 52	0.012 58	0.012 65		
$^3P_1$ $2s2p^*$	0.999 83	0.999 83		302.66	303.56
$2s2p$	0.018 34	0.018 36			
$^1P_1$ $2s2p^*$	−0.018 35		−0.018 37	4505.45	4503.26
$2s2p$	0.999 83		0.999 83		

TABLE II. Fitting coefficients for the excitation energies from the ground state. [The resulting energy is in eV. See Eq. (3).] The numbers in square brackets are powers of 10.

Coefficients	Excited states $2s2p\ ^3P_1$	$2s2p\ ^1P_1$
e_1	−3.784 87[+1]	1.080 85[+2]
e_2	6.771 75	−3.245 65[+1]
e_3	7.611 27[−1]	5.671 83
e_4	3.549 02[−2]	−7.249 07[−2]
e_5	−4.274 90[−6]	5.395 53[−5]
e_6	6.536 47[−10]	−1.697 52[−11]
e_7	−3.199 15[−14]	1.507 10[−13]

energies determined by using fully variational (relaxed) orbitals and those by using common (frozen) core orbitals. Table I indicates that the excitation energies are insensitive to the type of orbitals, more so for low-Z ions.

Experimental values of excitation energies for some ions are known, but it is not crucial to have a very accurate excitation energy to calculate cross sections. To help those cases for which experimental values are unknown, we fitted a power series in Z to the excitation energies E from the ground state to the $^3P_1$ and $^1P_1$ states calculated by the MCDF method

$$E = e_1/Z + e_2 + e_3 Z + e_4 Z^2 + e_5 Z^4 + e_6 Z^6 + e_7 Z^8 , \quad (3)$$

where the fitting coefficients e_i are listed in Table II. These coefficients reproduce the original excitation energies to better than 0.4% for $10 \le Z \le 92$.

In many cases, we had numerical convergence problems in distorted waves for incident energies too close to the threshold values. Hence cross sections were calculated to about 1.5 times the thresholds and then extrapolated to the thresholds by fitting to a quadratic equation. Partial waves for both incident and scattered electrons were calculated for $l \le 100$. Even then, partial-wave contributions did not converge sufficiently for high incident energies for low-Z ions. In such cases, we calculated the difference between corresponding plane-wave Born cross sections with and without partial wave expansions ($l \le 100$). This difference, which amounted to less than 30% of the total cross section in the most severe cases, was then added to the distorted-wave results with $l \le 100$.

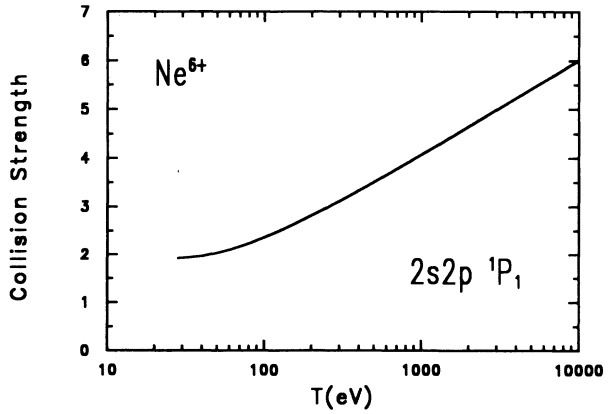

FIG. 1. Collision strength for the $2s^2 \rightarrow 2s2p\ ^1P_1$ excitation of Ne^{6+}. The incident energy (T) dependence illustrated here is a typical one for a spin- and electric dipole-allowed excitation.

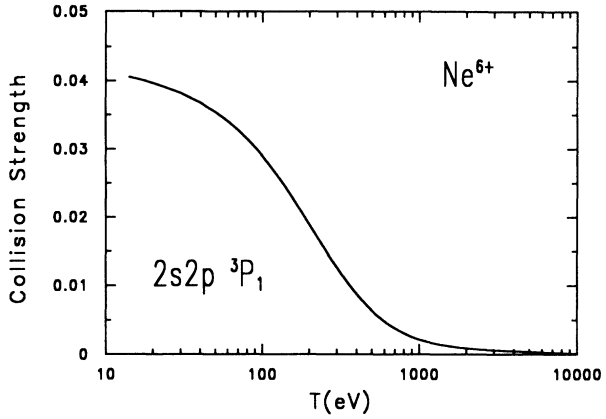

FIG. 2. Collision strength for the $2s^2 \rightarrow 2s2p\ ^3P_1$ excitation of Ne^{6+}. The incident energy (T) dependence presented here is a typical one for a spin- and electric dipole-forbidden excitation.

III. INCIDENT-ENERGY DEPENDENCE OF CROSS SECTIONS

As was reported elsewhere,[7] electron-impact cross section σ for a spin- and electric-dipole allowed excitation of an ion can be expressed as a compact function of the incident electron speed in units of the speed of light β and the incident energy T

$$\sigma = (\pi a_0^2 \alpha^2 / g_i \beta^2) S \quad (4)$$

with

$$S = [A \ln(T/H) + B + CH/T + D \ln(T/H)/(T/H)] , \quad (5)$$

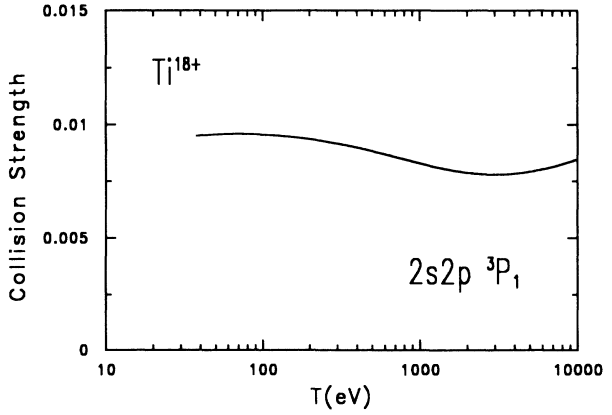

FIG. 3. Collision strength for the $2s^2 \rightarrow 2s2p\ ^3P_1$ excitation of Ti^{18+}. Intermediate coupling mixes the dipole-allowed ^1P component with the forbidden ^3P component. The ^1P component begins to alter the collision strength at high incident energy (T). [See Eq. (5).]

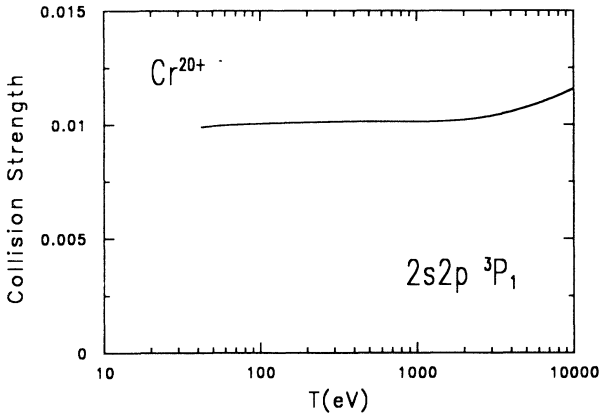

FIG. 4. Collision strength for the $2s^2 \rightarrow 2s2p\ ^3P_1$ excitation of Cr^{20+}. Mixing of allowed ^1P and forbidden ^3P components is strong enough to make the incident energy (T) dependence resemble neither an allowed nor a forbidden excitation.

where a_0 is the Bohr radius, α is the fine structure constant, g_i is the degeneracy of the initial state, S is the collision strength, H is the atomic unit of energy (=27.2114 eV), and A, B, C, and D are constants independent of T. These constants depend on the target ion as well as the type of transition. The particular form of T dependence in Eqs. (4) and (5) is based on nonrelativistic kinematics; a different form based on relativistic kinematics must be used for $T > 10$ keV.

Equation (5) is a modified form of the Bethe formula,[8] and A, B, C, and D are related to physical properties of the target ion. For instance, A is related to the dipole oscillator strength for the appropriate excitation and D is related to the ratio of the distorted-wave and plane-wave at the nucleus as well as to the dipole oscillator strength.[7]

The calculated collision strengths for the $2s^2 \rightarrow 2s2p\ ^1P_1$ excitations of Ne^{6+} through U^{88+} can easily be fitted by using Eq. (5). We found that the fitted values of D in Eq. (5) were sensitive to the collision strength values near thresholds. As was mentioned earlier, we extrapolated calculated values of S to appropriate thresholds to stabilize the values of D. A typical T dependence of the collision strength for a spin- and dipole-allowed transition is shown in Fig. 1.

For low-Z ions, the $2s^2 \rightarrow 2s2p\ ^3P_1$ excitation is spin-forbidden and the corresponding S has a very different T dependence from that for a spin- and dipole-allowed transition. We found that a function of the form

$$S = (A + BT/H)/(1 + CT/H + DT^2/H^2) \tag{6}$$

fitted calculated values of S for spin-forbidden excitations well,[7] where A, B, C, and D are fitting constants. Although Eq. (6) approaches T^{-1} for large T, the correct asymptotic behavior of S for a spin-forbidden excitation is known to be[9]

$$S \sim T^{-2} \text{ as } T \rightarrow \infty \ . \tag{7}$$

At present, the cause for this discrepancy in the asymptotic behavior of collision strength is not understood.

Intermediate coupling mixes the $^3P_1$ and $^1P_1$ states, and the T dependence of S for the $2s^2 \rightarrow 2s2p\ ^3P_1$ excitation gradually shifts toward that for the $2s2p\ ^1P_1$ excitation as Z increases. This shift in T dependence takes place in light ions and is almost completed by $Z=26$. As a consequence, we found that it was necessary to use a hybrid formula to fit S for the "forbidden" excitation, $2s^2 \rightarrow 2s2p\ ^3P_1$ for low-Z ions:

$$\begin{aligned} S(^3P_1, Z \le 26) &= A \ln(T/H) + B \\ &\quad + (C + DT/H)/[1 + ET/H + 0.01(T/H)^2] \ , \end{aligned} \tag{8}$$

where A, B, C, D, and E are fitting constants independent of T. The coefficient of the last term, 0.01, was chosen to maintain a uniform fitting accuracy for the entire range of Z we have used. The effect of intermediate coupling manifested as the shifting T dependence of S for the $2s^2 \rightarrow 2s2p2\ ^3P_1$ excitation is illustrated in Figs. 2–4.

IV. Z DEPENDENCE OF FITTING CONSTANTS

The constants in Eq. (5) are expected to have smooth Z dependence along an isoelectronic sequence because they are related to physical properties of the target ion. For instance, the constant A is related to the dipole oscillator strength divided by the excitation energy. Hence A is expected to vary as some inverse power of Z because the dipole oscillator strength is independent of Z (in nonrelativistic cases) and the excitation energy varies as some positive power of Z [see Eq. (3)]. In contrast, the precise relationship between the physical properties of the target ion and the constants in the Padé approximants of Eqs. (6) and (8) is not understood at present. Nevertheless, we

TABLE III. Fitting coefficients for the $2s2p\ ^3P_1$ excitation of Be-like ions, $Z \le 26$ [see Eqs. (8), (9a)–(9e)]. The numbers in square brackets are powers of 10.

Coefficient	$i=1$	2	3	4	5	6	Highest power
a_i	1.040 18[−3]	−6.436 66[−2]	1.586 19	−1.6746[+1]	6.220 37[+1]		Z
b_i	5.805 35[−6]	−7.667 18[−4]	3.784 92[−2]	−8.440 07[−1]	8.290 92	−2.888 71[+1]	Z^3
c_i	3.339 94[−3]	−2.268 56[−1]	5.992 30	−6.208 90[+1]	2.530 22[+2]		Z
d_i	2.180 73[−7]	5.290 33[−6]	−2.166 53[−3]	8.747 04[−2]	−1.095 33	4.218 19	Z^3
e_i	−4.416 94[−4]	3.600 30[−2]	−1.141 00	1.883 39[+1]	−1.562 18[+2]	5.096 92[+2]	Z^3

found that the fitting constants in Eq. (8) exhibited smooth Z dependence along the Be isoelectronic sequence.

We took advantage of this smooth Z dependence of the fitted constants and expressed them in terms of simple functions of Z. Such functions allow one to determine the values of the fitting constants A, B, etc. for an arbitrary ion, and then to evaluate excitation cross sections at desired incident energies using Eqs. (5) or (8).

For the $^3P_1$ excitation of ions with $10 \le Z \le 26$, the fitting constants in Eq. (8) are given by

$$A = a_1 Z + a_2 + a_3/Z + a_4/Z^2 + a_5/Z^3 , \quad (9a)$$

$$B = b_1 Z^3 + b_2 Z^2 + b_3 Z + b_4 + b_5/Z + b_6/Z^2 , \quad (9b)$$

$$C = c_1 Z + c_2 + c_3/Z + c_4/Z^2 + c_5/Z^3 , \quad (9c)$$

$$D = d_1 Z^3 + d_2 Z^2 + d_3 Z + d_4 + d_5/Z + d_6/Z^2 , \quad (9d)$$

$$E = e_1 Z^3 + e_2 Z^2 + e_3 Z + e_4 + e_5/Z + e_6/Z^2 , \quad (9e)$$

where a_i, b_i, c_i, etc. are given in Table III. With Eqs. (8), (9a)–(9e), and Table II, we could reproduce our calculated values of S within 2% for any Be-like ion with $10 \le Z \le 26$ from threshold to $T = 10$ keV for the $2s^2\,{}^1S_0 \rightarrow 2s2p\,{}^3P_1$ excitation by electron impact.

Meanwhile, for the $2s^2 \rightarrow 2s2p\,{}^1P_1$ excitation of ions with $10 \le Z \le 26$, one can use Eq. (5) with

$$A = a_1/Z + a_2/Z^2 + a_3/Z^3 , \quad (10a)$$

$$B = b_1 \exp(-Z/200) + b_2 + b_3/Z + b_4/Z^2 , \quad (10b)$$

$$C = c_1 Z^3 + c_2 Z^2 + c_3 Z + c_4 , \quad (10c)$$

$$D = d_1 Z^2 + d_2 Z + d_3 + d_4/Z + d_5/Z^2 + d_6/Z^3 , \quad (10d)$$

The values of a_i, b_i, c_i, and d_i are listed in Table IV.

For $Z \ge 26$, both the $^3P_1$ and $^1P_1$ states become almost pure jj states, the former approaching a pure $2s_{1/2}2p_{1/2}$ configuration while the latter becoming an almost pure $2s_{1/2}2p_{3/2}$ configuration. Excitations to both states become spin and dipole allowed and hence Eq. (5) is appropriate to fit relevant collision strengths.

For the excitation to the lower $J = 1$ state (nominally $^3P_1$ state) of ions with $Z \ge 26$, the constants in Eq. (5) are given by

$$A = a_1 Z + a_2 + a_3/Z + a_4/Z^2 + a_5/Z^3 , \quad (11a)$$

$$B = b_1 Z^2 + b_2 Z + b_3 + b_4/Z + b_5/Z^2 + b_6/Z^3 , \quad (11b)$$

$$C = c_1 Z^2 + c_2 Z + c_3 + c_4/Z + c_5/Z^2 + c_6/Z^3 , \quad (11c)$$

$$D = (d_1 + d_2 Z)/(1 + d_3 Z + d_4 Z^2) , \quad (11d)$$

where the values of a_i, b_i, c_i, and d_i are listed in Table V.

Finally, for the excitation to the upper $J = 1$ state (nominally $^1P_1$ state) of ions with $Z \ge 26$, Eq. (5) should be used with

$$A = a_1/Z + a_2/Z^2 + a_3/Z^3 , \quad (12a)$$

$$B = b_1 \exp(-Z/200) + b_2 Z + b_3 + b_4/Z + b_5/Z^2 , \quad (12b)$$

$$C = c_1 Z^3 + c_2 Z^2 + c_3 Z + c_4 , \quad (12c)$$

$$D = d_1 Z + d_2 + d_3/Z . \quad (12d)$$

The values of a_i, b_i, c_i, and d_i are given in Table VI. All constants in Tables III–VI are chosen such that the atomic unit of energy (hartree = 27.2114 eV) should be used with Eqs. (5) and (8).

V. DISCUSSION

It is known that the mixing among the configurations that are degenerate in the hydrogenic limit will not diminish as Z increases. The ground state of Be-like ions is such a case since $2s^2$ and $(2p_{1/2})^2$ are degenerate in the hydrogenic limit (see Table I). In order to study the importance of configuration mixing, both singlet and triplet excitation cross sections were calculated for Ne^{6+}, Fe^{22+}, and Xe^{50+} using a single-configuration wave function for the ground state, i.e., only the $2s^2$ configuration was used for the ground state. The excited states were still represented by a mixture of the $2s2p_{1/2}$ and $2s2p_{3/2}$ configuration to retain intermediate coupling. As is illustrated in Figs. 5–7, single-configuration results are larger by 10–60% than the corresponding multiconfiguration results. This difference is larger for the $2s2p\,{}^3P_1$ excitations than for the $2s2p\,{}^1P_1$ excitations (see Table VII) probably because the former is the weaker of the two and hence more sensitive to changes in mixing coefficients and transition-matrix elements. In addition, the lower $J = 1$ level ($^3P_1$) consists of nearly pure $2s2p_{1/2}$ configuration for high Z while, in the ground state, the mixing of the $(2p_{1/2})^2$ configuration is much more important than that of the $(2p_{3/2})^2$ configuration (see Table I). This in turn introduces a stronger interaction between the ground state and the lower $J = 1$ level than between the ground state and the upper $J = 1$ level. Thus the cross section for the $^3P_1$ excitation is more sensitive to the configuration mixing than that for the $^1P_1$ excitation. The T dependence of the ratio of multiconfiguration and single-configuration results for the triplet excitation of Ne^{6+}, however, exhibits a trend totally different from the rest; the single-configuration results are smaller than the multiconfiguration results for low T but the trend is reversed for $T \approx 2$ keV and above.

The distorted-wave Born cross sections for Fe^{22+} calculated by Mann[10] are based on a method similar to ours except for the fact that he used nonrelativistic wave functions both for the target ion and for continuum orbitals. Spin-orbit interaction is introduced as a perturbation. We compare his results with ours in Figs. 5 and 8. Mann's results for the $^1P_1$ excitation in Fig. 5 are in close agreement with ours because relativistic effects are not yet dominant at $Z = 26$. In Fig. 7, we compare our relativistic collision strengths for the $^3P_0$, $^3P_1$, and $^3P_2$ excitations with those calculated by Bhatia and Mason.[11] They used distorted-wave codes developed by the University College London with correlated but nonrelativistic target wave functions. Their $^3P_0$ and $^3P_2$ collision strengths are practically the same as ours. Their $^3P_1$ collision strengths, curve (e) in Fig. 7, are similar to our values, curve (d), but their T dependence is qualitatively different from that observed in our result. Norrington

TABLE IV. Fitting coefficients for the $2s2p\ ^1P_1$ excitation of Be-like ions, $Z \leq 26$ [see Eqs. (5), (10a)–(10d)]. The numbers in square brackets are powers of 10.

Coefficient	$i=1$	2	3	4	5	6	Highest power
a_i	4.150 66[−1]	5.750 13[+1]	2.3740[+2]				Z^{-1}
b_i	4.798 07	−3.368 99	−3.610 19[+1]	3.375 39[+2]			$\begin{cases}\exp\\ Z^0\end{cases}$
c_i	−9.232 88[−6]	1.241 42[−3]	−7.831 53[−2]	1.631 86			Z^3
d_i	−3.029 42[−3]	3.414 51[−1]	−1.438 03[+1]	3.027 74[+2]	−2.919 06[+3]	1.026 82[+4]	Z^2

TABLE V. Fitting coefficients for the lower $J=1$ ($2sp2\ ^3P_1$) excitation of Be-like ions, $Z \geq 26$ [see Eqs. (5), (11a)–(11d)]. The numbers in square brackets are powers of 10.

Coefficient	$i=1$	2	3	4	5	6	Highest power
a_i	2.502 39[−4]	−6.405 87[−2]	5.606 64	−1.703 28[+2]	1.673 93[+3]		Z
b_i	−1.878 98[−5]	5.041 53[−3]	−4.997 98[−1]	2.224 06[+1]	−4.566 44[+2]	3.663 00[+3]	Z^2
c_i	4.464 66[−5]	−1.009 03[−2]	7.223 17[−1]	−2.134 37[+1]	2.819 97[+2]	−1.464 63[+3]	Z^2
d_i	−1.818 53[−2]	7.928 56[−4]	−2.591 81[−2]	3.700 65[−4]			Padé

TABLE VI. Fitting coefficients for the upper $J=1$ ($2s2p\ ^1P_1$) excitation of Be-like ions, $Z \geq 26$ [see Eqs. (5), (12a)–(12d)]. The numbers in square brackets are powers of 10.

Coefficient	$i=1$	2	3	4	5	Highest power
a_i	−8.217 15[−1]	1.127 24[+2]	−3.232 52[+2]			Z^{-1}
b_i	−1.170 17	−3.384 57[−3]	1.065 41	−3.530 37	9.026 03[+1]	$\begin{cases}\exp\\ Z\end{cases}$
c_i	−2.885 34[−6]	4.911 09[−4]	−4.873 35[−2]	1.236 79		Z^3
d_i	9.464 63[−4]	3.368 27[−1]	−7.138 18[−4]			Z

TABLE VII. Comparison of single-configuration (SCDF) and multiconfiguration Dirac-Fock (MCDF) results. Directly calculated collision strengths are listed here. These values may be slightly different from those derived from the fitted coefficients in Tables III–VI. The numbers in square brackets are powers of 10.

Ion	Incident energy (eV)	$^3P_1$ Collision strengths MCDF	$^3P_1$ Collision strengths SCDF	$^1P_1$ Collision strengths MCDF	$^1P_1$ Collision strengths SCDF
Ne^{6+}	100	2.886[−1]	2.547[−2]	2.344	3.455
	500	6.500[−3]	5.620[−3]	3.504	5.144
	1000	2.408[−3]	2.184[−3]	4.093	6.038
	5000	3.200[−4]	4.889[−4]	5.430	8.014
	10 000	2.425[−4]	4.437[−4]	5.969	8.808
Fe^{22+}	500	1.172[−2]	1.728[−2]	3.585[−1]	4.822[−1]
	1000	1.225[−2]	1.878[−2]	4.097[−1]	5.512[−1]
	5000	1.400[−2]	2.322[−2]	5.698[−1]	7.659[−1]
	10 000	1.519[−2]	2.550[−2]	6.395[−1]	8.601[−1]
Xe^{50+}	1000	1.953[−2]	2.770[−2]	5.884[−2]	6.584[−2]
	5000	2.586[−2]	3.702[−2]	7.484[−2]	8.370[−2]
	10 000	2.919[−2]	4.190[−2]	8.583[−2]	9.620[−2]

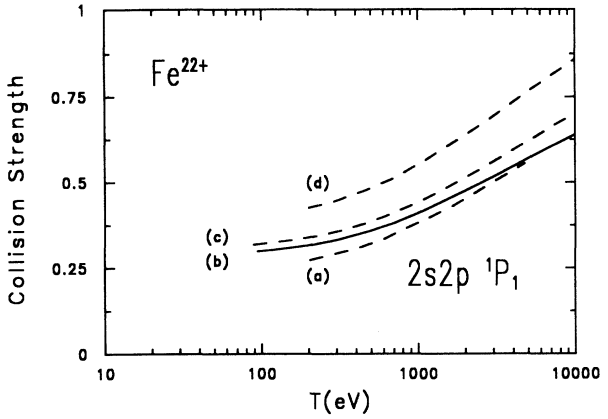

FIG. 5. Collision strengths for the $2s^2 \rightarrow 2s2p\ ^1P_1$ excitation of Fe^{22+}. Curve (a), nonrelativistic distorted-wave Born results calculated by Bhatia and Mason (Ref. 11) using correlated nonrelativistic wave functions; curve (b), our result calculated by using a multiconfiguration Dirac-Fock wave function for the ground state; curve (c), nonrelativistic distorted-wave Born collision strength calculated by Mann (Ref. 10) using correlated nonrelativistic wave functions; curve (d), our results obtained by using a single-configuration Dirac-Fock wave function for the ground state.

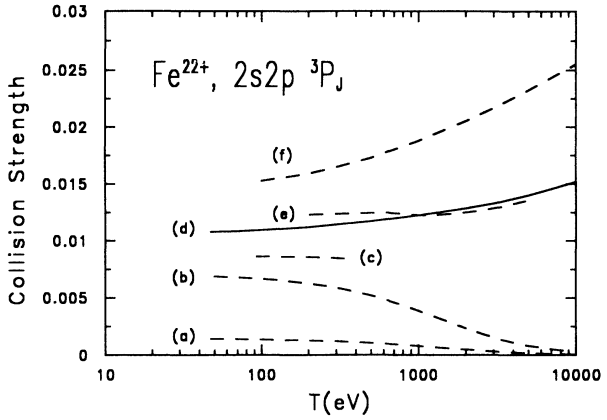

FIG. 7. Collision strengths for the $2s^2 \rightarrow 2s2p\ ^3P_J$ excitation of Fe^{22+}. Curve (a), our collision strength for the $2s^2 \rightarrow 2s2p\ ^3P_0$ excitation; curve (b), our result for the $^3P_2$ excitation; curve (c), collision strength for the $^3P_1$ excitation from a five-state relativistic R-matrix calculation by Norrington and Grant (Ref. 12); curve (d), the present result for the $^3P_1$ excitation obtained by using MCDF wave functions; curve (e) nonrelativistic collision strength of the $^3P_1$ excitation calculated by Bhatia and Mason (Ref. 11); curve (f), our relativistic distorted-wave Born result for the $^3P_1$ excitation calculated using a single-configuration Dirac-Fock wave function for the ground state.

and Grant[12] calculated the $^3P_1$ collision strength using a relativistic R-matrix method that included five states. Their result, curve (c) in Fig. 7, is substantially lower than our corresponding result. Norrington and Grant suggest that the coupling to the $^1P_1$ channel reduces the $^3P_1$ cross section. Were this the case, then the $^1P_1$ cross section based on the same relativistic R-matrix method should be greater than our $^1P_1$ cross section. At present, $^1P_1$ excitation cross section based on relativistic R-matrix method is not available in the literature.

Although Mann[10] accounted for intermediate coupling, his result for the ^3P excitation cannot be directly compared with ours because his ^3P collision strength corresponds to the sum of our $^3P_0$, $^3P_1$, and $^3P_2$ collision strengths. In Fig. 8, we compare Mann's results[10] for the ^3P excitation with the sum of our three ^3P_J results, as well as the sum of the ^3P_J results by Bhatia and Mason.[11] The sharp rise near the threshold for the ^3P excitation in our result, curve (a) of Fig. 8, is caused by the opening of the $^3P_2$, excitation channel as the incident energy is increased. Once all ^3P_J channels become open as T is in-

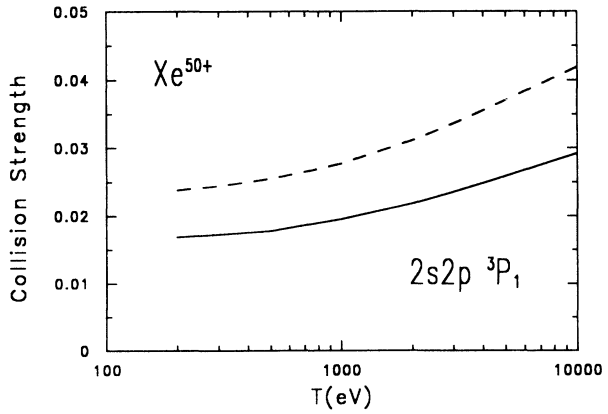

FIG. 6. Collision strengths for the $2s^2 \rightarrow 2s2p\ ^3P_1$ excitation of Xe^{50+}. The solid curve represents our multiconfiguration result and the dashed curve stands for our single-configuration results.

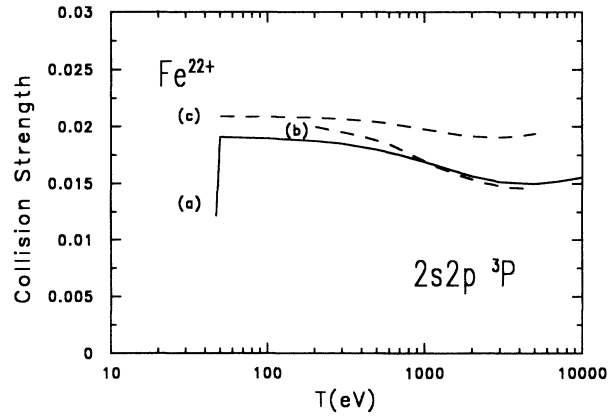

FIG. 8. Sum of the collision strengths for the $2s^2 \rightarrow 2s2p\ ^3P_J$ excitation of Fe^{22+}. Curve (a), our result calculated by using MCDF wave functions; curve (b), result obtained by Bhatia and Mason (Ref. 11) using correlated nonrelativistic wave functions; curve (c), collision strength calculated by Mann (Ref. 10) using correlated nonrelativistic wave functions. The sharp rise in curve (a) near the threshold indicates that a new channel ($^3P_2$) is allowed when the incident energy is increased.

creased, Mann's nonrelativistic collision strength is 10–20 % larger than our correlated relativistic result. In Ref. 10, Mann used scaled F_k and G_k integrals to determine target wave functions. Later, he repeated his calculations without such scaling,[13] and obtained results which are very close to our relativistic results. This scaling, commonly known as the Cowan scaling of Slater integrals, is introduced to obtain energy levels closer to experimental data. However, the question of whether such a scaling would produce more reliable collision cross sections has not been answered in any definitive way. We simply caution that use of the Cowan scaling could change collision strengths by 10–20 %, primarily by changing the degree of configuration mixing and intermediate coupling. Forbidden transitions are expected to be more sensitive to the Cowan scaling because they are more sensitive to configuration mixing.

The T dependence of the $^3P_1$ and $^1P_1$ collision strengths by Bhatia and Mason[11] [curve (a) of Fig. 5 and curve (e) of Fig. 7] shows opposite trends when compared to ours. This is an indication that the intermediate coupling used in Ref. 11 to separate the $^3P_1$ and $^1P_1$ cross sections disagrees with our result, which accounts for the change in the ratio of the two cross sections as a function of the incident energy.

Bhatia and Feldman published[14] collision strengths for the ^3P and ^1P excitations of Kr^{32+} calculated by using the University College London codes. Again, wave functions used by them are nonrelativistic, but relativistic corrections on energies and intermediate coupling have been introduced, and distorted-wave Born cross sections were calculated from them. Their results are compared with ours in Table VIII. Our results were obtained by using the fitted constants in Tables II, V, and VI. It is likely that the $^1P_1$ collision strength reported by Bhatia and Feldman is lower than ours by 10–20 % because their partial-wave expansion was insufficient ($l < 8$), though they used a Coulomb-Bethe procedure to extrapolate their results to higher l. On the other hand, their $^3P_1$ result agrees well with ours.

We also calculated collision strengths for Fe^{22+} by using the J-specific exchange terms with the core electrons instead of the jj-configuration average exchange terms, but the results were hardly changed (1–2 % at the most) from those based on the configuration average exchange. Moreover, for highly charged ions, distorted waves obtained without any exchange terms with core electrons led to collision strengths nearly the same (again 1–2 % difference at the most) as those obtained with exchange terms. Omitting orthogonality constraints between bound and continuum orbitals also has minimal effect in resulting cross sections. Omission of the exchange terms and the orthogonality constraints in solving Dirac-Fock equations for the distoted waves usually saves computer time by almost an order of magnitude.

On the other hand, the exchange terms in the interaction matrix element, which are equivalent to the Born-Oppenheimer terms in the plane-wave Born approximation, reduce collision strengths by 10% or more in many cases. These exchange terms are significant only for distorted waves with low κ ($|\kappa| \leq 10$) and their magnitudes are somewhat sensitive to the orthogonality of the distorted waves with bound orbitals of the same κ.

One drawback of the distorted-wave Born approximation, both in relativistic and nonrelativistic versions, is the absence of coupling of the final state to other multiply excited states of the same J and parity. Such a coupling, which is equivalent to configuration mixing of the combined system, i.e., the incident electron plus the target ion, with multiply excited, quasibound states, will lead to resonances near excitation thresholds. A large number of resonances could raise the average cross section close to such thresholds. In other words, the disorted-wave Born approximation is still a first-order perturbation theory and it cannot adequately account for strong coupling between different modes of excitations near the appropriate thresholds. In this sense, one must be cautious in applying our results for incident energies very close to thresholds.

VI. CONCLUSIONS

By using multiconfiguration Dirac-Fock wave functions to describe target ions and relativistic distorted waves for the incoming and outgoing electron, we are able to account for electron correlation, intermediate coupling, and other relativistic effects in the collision cross sections for the excitation of Be-like ions by electron impact. Moreover, collision strengths were fitted to simple functions of the incident energy T with four or five fitting constants, Eqs. (5) and (8), depending on whether the excitation is electric-dipole and spin allowed or not. These fitting constants were found to have smooth Z dependence, and they were in turn fitted to simple powers of Z, Eqs. (9)–(12). Associated excitation energies are also given as a power series of Z, Eq. (3). These fitted constants, which total less than 100, provide accurate reproduction of the original relativistic distorted-wave

TABLE VIII. Comparison of collision strengths for Kr^{32+}.

Incident energy[a]	$^3P_1$ excitation		$^1P_1$ excitation	
	Present work	Reference 14	Present work	Reference 14
12.5	0.018 94	0.019 36	0.1559	0.1286
20	0.020 06	0.020 36	0.1639	0.1393
30	0.021 28	0.021 46	0.1739	0.1522
40	0.022 27	0.022 41	0.1826	0.1635

[a]In hartree (=27.2114 eV).

Born cross sections from thresholds to $T=10$ keV for arbitrary ions from Ne^{6+} through U^{88+}. These compact expressions should be useful in plasma modeling as well as in the determination of cross sections for individual ions as needed.

We found that the cross section for the $2s^2 \rightarrow 2s2p\ ^3P_1$ excitation is much more sensitive to configuration mixing than the corresponding $^1P_1$ excitation cross section. We also found that the distorted-wave cross sections obtained with short expansions of partial waves (e.g., Ref. 14) are likely to be too small even if a Coulomb-Bethe procedure is used to account for the truncated expansion.

One advantage of a relativistic formulation is that configuration mixing and intermediate coupling are treated on equal footing, while in a nonrelativistic formulation intermediate coupling must be treated as a perturbation. The advantage of a relativistic formulation will become more apparent for medium to heavy ions in which intermediate coupling becomes more important than configuration mixing. For instance, the ratios of the three ^3P_J excitation cross sections (for $J=0$, 1, and 2) do not follow those of statistical weights; the ratios are dependent on T and sensitive to the intermediate coupling between the $^1P_1$ and $^3P_1$ states. A nonrelativistic calculation will not be able to provide reliable ratios as functions of T [see curve (b) of Fig. 5 and curve (e) of Fig. 7].

For highly charged ions, our experience shows that considerable savings in computer time can be achieved without sacrificing much accuracy (1–2 % at the most) by omitting the exchange terms with core orbitals in solving Dirac-Fock equations for distorted waves. Cross sections, however, are much more sensitive to the exchange terms in the interaction matrix element.

The procedure illustrated in this article in getting compact expressions for cross sections for all members of an isoelectronic sequence should be applicable to a wide range of electron-ion collision processes, and it should simplify the task of storing and retrieving cross section data in applications that require a wide variety and large number of such cross sections.

ACKNOWLEDGMENTS

This work was supported in part by the Office of Fusion Energy, U.S. Department of Energy, Lawrence Livermore National Laboratory, and by the North Atlantic Treaty Organization Scientific Research Grant No. 85/0744. Two of us (Y.K.K. and J.P.D.) carried out part of this work at the Institute for Theoretical Physics, University of California, Santa Barbara. The research at the Institute was supported in part by the National Science Foundation under Grant No. PHY82-17853, supplemented by funds from the National Aeronautics and Space Administration. We are also grateful to Dr. J. B. Mann for providing us with his theoretical data which were indispensable in verifying our codes.

*Permanent address: Physics Department, Liaoning University, Shenyang, People's Republic of China.

[1]Y.-K. Kim and J. P. Desclaux, Phys. Scr. **36**, 796 (1987).
[2]C. Møller, Ann. Phys. (Leipzig) **14**, 531 (1932). (1986).
[3]P. L. Hagelstein, Phys. Rev. A **34**, 874 (1986).
[4]J. P. Desclaux, Comput. Phys. Commun. **9**, 31 (1975).
[5]A. W. Weiss, Phys. Rev. **122**, 1826 (1961).
[6]D. R. Hartree, Proc. Roy. Soc. London, Ser. A **154**, 588 (1936).
[7]Y.-K. Kim and J. P. Desclaux, Phys. Rev. A **38**, 1805 (1988).
[8]Y.-K. Kim and M. Inokuti, Phys. Rev. A **3**, 665 (1971).
[9]M. H. Mittleman, Phys. Rev. **164**, 48 (1967).
[10]J. B. Mann, At. Data Nucl. Data Tables **29**, 407 (1983).
[11]A. K. Bhatia and H. E. Mason, Astron. Astrophys. **155**, 413 (1986).
[12]P. H. Norrington and I. P. Grant, J. Phys. B **20**, 4869 (1987).
[13]J. B. Mann (private communication).
[14]A. K. Bhatia and U. Feldman, J. Appl. Phys. **53**, 4711 (1982).